HHS Public Access

Author manuscript

Nat Med. Author manuscript; available in PMC 2017 July 01.

Published in final edited form as:

Nat Med. 2017 January ; 23(1): 39–48. doi:10.1038/nm.4240.

Thalamic miR-338-3p mediates auditory thalamocortical disruption and its late onset in 22q11.2 microdeletion models

Sungkun Chun[1,#,+], **Fei Du**[1,#,!], **Joby J. Westmoreland**[1,#,^], **Seung Baek Han**[1], **Yong-Dong Wang**[2], **Donnie Eddins**[1], **Ildar T. Bayazitov**[1], **Prakash Devaraju**[1], **Jing Yu**[1], **Marcia M. Mellado Lagarde**[1], **Kara Anderson**[1], and **Stanislav S. Zakharenko**[1,*]

[1]Department of Developmental Neurobiology, St. Jude Children's Research Hospital, Memphis, TN 38105, USA

[2]Department of Computational Biology, St. Jude Children's Research Hospital, Memphis, TN 38105, USA

Abstract

Although 22q11.2 deletion syndrome (22q11DS) is associated with early-life behavioral abnormalities, affected individuals are also at high risk for the development of schizophrenia symptoms, including psychosis, later in life. Auditory thalamocortical projections recently emerged as a neural circuit specifically disrupted in 22q11DS mouse models, in which haploinsufficiency of the microRNA-processing gene *Dgcr8* resulted in the elevation of the dopamine receptor Drd2 in the auditory thalamus, an abnormal sensitivity of thalamocortical projections to antipsychotics, and an abnormal acoustic-startle response. Here we show that these auditory thalamocortical phenotypes have a delayed onset in 22q11DS mouse models and are associated with an age-dependent reduction of the microRNA miR-338-3p, which targets *Drd2* and is enriched in the thalamus of both humans and mice. Replenishing depleted miR-338-3p in mature 22q11DS mice rescued the thalamocortical abnormalities, and miR-338-3p deletion/knockdown mimicked thalamocortical and behavioral deficits and eliminated their age dependence. Therefore, miR-338-3p depletion is necessary and sufficient to disrupt auditory thalamocortical signaling in 22q11DS mouse models and may mediate the pathogenic mechanism of 22q11DS-related psychosis and control its late onset.

[*]Correspondence should be addressed to S.S.Z. (stanislav.zakharenko@stjude.org).
[#]These authors contributed equally to this work.
[+]Present address: Department of Physiology, Chonbuk National University Medical School, South Korea
[!]Present address: Channing Division of Network Medicine, Bringham and Women's Hospital, Boston, MA, 02115, USA
[^]Present address: Department of Cell and Molecular Biology, Tulane University, New Orleans, LA, 70118, USA

CONTRIBUTIONS

S.S.Z., J.J.W, F.D., and S.C. designed the research; S.C. performed whole-cell recordings; F.D., J.J.W., and S.B.H. designed and constructed microRNA molecular tools and verified these tools in vitro and in vivo; Y.-D.W. performed microRNA array analysis; I.T.B. and P.D. performed 2-photon imaging and whole-cell recordings; J.Y. and K.A. assisted with qRT-PCR and Western blotting; D.E. and M.M.M.L. performed mouse behavior experiments; S.S.Z. wrote the paper with help from the other authors.

Conflict of Interest

The authors declare no conflict of interest.

Introduction

Thalamocortical (TC) projections to the auditory cortex (ACx), a brain region implicated in auditory hallucinations[1–4], have emerged as a circuit specifically disrupted[5] in mouse models of 22q11.2 deletion syndrome (22q11DS)[6]. This disorder, the most common microdeletion syndrome in humans[7, 8], is caused by a hemizygous microdeletion (1.5–3 Mb) on the long arm of chromosome 22[9]. The 22q11DS is considered a leading genetic cause of schizophrenia[10–12]. Schizophrenia develops in 23% to 43% of individuals with 22q11DS[13–18], most of whom experience psychosis[19, 20]. Furthermore, 30% to 50% of nonschizophrenic individuals with 22q11DS demonstrate subthreshold symptoms of psychosis[21]. Nonpsychotic behavioral abnormalities are present from early life in patients with 22q11DS[22, 23], but psychotic symptoms and schizophrenia are delayed; the median age of psychosis onset is 21 years[18, 24, 25]. In schizophrenic patients, auditory hallucinations and other psychotic symptoms are similarly delayed until late adolescence or early adulthood[26, 27], are present in 60% to 90% of cases[28], and are often alleviated by antipsychotics that inhibit D2 dopamine receptors (DRD2s)[29, 30]. Given the germline occurrence of deleted genes in 22q11DS, it is unclear why the onset of positive symptoms is delayed.

Recently, *Dgcr8* emerged as a culprit gene responsible for several neuronal phenotypes in mouse models of 22q11DS[31, 32], including the disruption of synaptic transmission at TC projections to the ACx[5]. Dgcr8 is part of the microprocessor complex that mediates the biogenesis of microRNAs (miRNAs), small RNAs that negatively regulate the expression of complementary mRNAs and protein translation[33]. *Dgcr8* haploinsufficiency in 22q11DS leads to depletion of miRNAs and the resultant upregulation of respective targets, which in turn disrupts synaptic transmission, synaptic plasticity, and proper functioning of neural circuits[34]. In adult 22q11DS mouse models, *Dgcr8* haploinsufficiency is sufficient to upregulate Drd2 mRNA and protein in the auditory thalamus, causing auditory abnormalities that include decreased glutamatergic synaptic transmission at TC projections to the ACx and deficient prepulse inhibition (PPI) of the acoustic-startle response[5]. Abnormally high levels of Drd2 in the thalamus of 22q11DS mice increase TC projection sensitivity to Drd2 antagonists, including antipsychotics. As a consequence, auditory synaptic and behavioral abnormalities of 22q11DS mice are rescued by antipsychotics[5].

Here we tested whether TC disruption follows the same age-dependent trajectory as psychosis in patients with 22q11DS or schizophrenia and determined the molecular underpinnings of TC disruption in 22q11DS mice.

Results

Delayed disruption of TC synaptic transmission in 22q11DS models

We compared basal synaptic transmission in young (2-month-old) and mature (4-month-old) *Df(16)1/+* mice, a murine model of 22q11DS[6] (Fig. 1a), and their wild-type (WT) littermates. Mice between the age of 3 and 6 months correspond to mature human adults between the age of 20 and 30 years[35]. Using whole-cell voltage-clamp recordings, we measured TC excitatory postsynaptic currents (EPSCs) from thalamorecipient ACx cortical

layer (L) 3/4 pyramidal neurons[36], while stimulating TC projections in acute brain slices containing the auditory thalamus (i.e., the ventral part of the medial geniculate nuclei [MGv]) and the ACx (Fig. 1b). The input–output relationship between stimulation intensity and TC EPSC, a measure of basal synaptic transmission at TC projections, was deficient in older but not younger mutant mice compared to WT controls (Fig. 1c,d). Consistent with the notion that the Drd2 elevation in thalamic-relay neurons reduces glutamatergic synaptic transmission at auditory TC projections in *Df(16)1/+* mice[5], the *Drd2* mRNA level was elevated in the MGv of older but not younger *Df(16)1/+* mice (Fig. 1e).

Elevated Drd2 levels in older *Df(16)1/+* mice mediate the abnormal sensitivity of mutant TC projections to antipsychotics; thus, we tested the time course of this sensitivity at different ages (1.5–7 months). In brief, we stimulated the thalamic radiation of WT mice to evoke TC EPSCs with a rise slope of approximately 100 pA/ms. We compared the effect of the antipsychotic agent haloperidol on TC EPSC 30 min after its bath application (1 μM) to the preapplication baseline TC EPSC (ΔH, a measure of haloperidol sensitivity). We determined that ΔH was significantly higher in *Df(16)1/+* mice than in WT littermates but only beginning at 3 months of age (Fig. 1f–h). In older mice, a similar intensity of thalamic stimulation (see Online Methods) evoked substantially smaller TC EPSCs in *Df(16)1/+* mice compared to WT controls, and haloperidol rescued that deficit (Fig. 1g). In contrast, TC projections in younger mutant mice were not sensitive to haloperidol (Fig. 1f,h).

Consistent with the notion that *Dgcr8* underlies the TC deficiency in 22q11DS[5], TC projections in *Dgcr8*$^{+/-}$ mice older than 3 months were sensitive to haloperidol, while those in WT mice were not. TC projections in younger mice were not sensitive to haloperidol (Fig. 1i–k). *Drd2* mRNA levels were also elevated in the thalamus of only the older *Dgcr8*$^{+/-}$ mice (Fig. 1l). Furthermore, PPI, a measure of sensorimotor gating that is typically reduced in schizophrenic patients[37, 38], was deficient in older but not younger *Dgcr8*$^{+/-}$ mice (Fig. 1m,n).

miR-338-3p mediates the disruption of TC synaptic transmission in 22q11DS

Because Dgcr8 mediates miRNA processing[33], we sought to identify the miRNA(s) mediating the *Dgcr8–Drd2* mechanism of TC deficiency. To this end, we performed miRNA microarray analysis of the auditory thalamus of 2- and 4-month-old mice (Table S1). Among the miRNAs that potentially target the *Drd2* transcript (based on miRWalk and Exiqon miRNA target–prediction algorithms), only five miRNAs (miR-337-3p, miR-337-5p, miR-335-5p, miR-335-3p, and miR-338-3p) were depleted in the auditory thalamus of *Df(16)1/+* or *Dgcr8*$^{+/-}$ mice (Fig. 2a–d). Because miR-185, which is not a *Drd2*-targeting miRNA, is encoded within the *Df(16)1* microdeletion, its depletion in *Df(16)1/+* mice served as a positive control (Fig. 2a,b). The qRT-PCR analysis verified that all five *Drd2*-targeting miRNAs were depleted in *Dgcr8*$^{+/-}$ mice (Fig. S1a). The expression of miRNAs decreased with age, regardless of genotype. The miRNA levels in older mice were lower than those in young WT or *Dgcr8*$^{+/-}$ mice. However, because *Dgcr8* haploinsufficiency depleted these miRNAs at both ages, the age-dependent decline in miRNA expression was exacerbated in mutants and reached minimal values at 4 months in *Dgcr8*$^{+/-}$ mice (Fig. S1a). Of the five miRNAs predicted to target Drd2 overexpression, miR-337-3p, miR-337-5p,

miR-335-3p, and miR-338-3p but not miR-335-5p decreased *DRD2* mRNA in vitro in human SH-SY5Y cells (Fig. S1b).

To identify which miRNA(s) targeting the *Drd2* 3′UTR (Fig. 2e) regulates the *Dgcr8–Drd2* mechanism of TC deficiency in vivo, we performed a screen based on the abnormal sensitivity of TC projections to haloperidol. We overexpressed mature miRNAs in excitatory thalamic neurons by injecting adeno-associated viruses (AAVs) encoding GFP with miR-337-5p, miR-338-3p, miR-335-5p, miR-337-3p, or miR-335-3p, under the control of excitatory neuron–specific promoter *CamKIIα* into the MGv of *Df(16)1/+* and WT mice (Fig. 2f,g). Overexpression of individual miRNAs in 4-month-old *Df(16)1/+* mice not only replenished the depleted miRNA levels but also elevated them beyond those in WT mice (Fig. S2a–e). However, of the five miRNAs, only miR-338-3p overexpression rescued the abnormal haloperidol sensitivity in *Df(16)1/+* mice (Figs. 2h, S2f–k). Overexpression of miR-338-3p in the MGv of *Df(16)1/+* mice decreased *Drd2* mRNA levels in the MGv by 47.6% ± 10.2% compared to the control virus (n = 6 mice for *AAV-GFP-miR-338-3p* and 6 mice for *AAV-GFP*; $p < 0.01$), confirming that miR-338-3p regulates *Drd2* levels.

The miR-338-3p, miR-335-3p, and miR-335-5p have conserved seed sites in the mouse and human *Drd2* 3′UTR. Consistent with the notion that only abundant miRNAs effectively regulate the targeting transcript(s)[39], miR-338-3p appeared to be more crucial for *Drd2* regulation in the auditory thalamus than did miR-337-5p, miR-335-5p, miR-337-3p, or miR-335-3p. Indeed, miR-338-3p was enriched in the thalamus compared to the other four miRNAs; miR-337-3p, miR-335-5p, miR-337-3p, and miR-335-3p levels were approximately 0% to 1% that of miR-338-3p (Fig. 2i). Moreover, miR-338-3p was enriched in the thalamus compared to other tested brain regions (Fig. 2i), suggesting that depletion of this *Drd2*-regulating miRNA in 22q11DS mainly affects thalamic function. Similarly, miR-338-3p was enriched in the MGv compared to the ACx (Brodmann area 41) in postmortem tissue samples from human subjects (n=7 for the MGv and n=8 for the ACx, $p<0.001$) (Fig. 2j and Table S2). Moreover, miR-338-3p was significantly decreased in the thalamus but not the ACx of schizophrenic patients compared to that in age- and sex-matched controls (Fig. 2j). We previously showed that the DRD2 protein level is elevated in MGv samples[5].

Replenishing miR-338-3p in the MGv rescues the TC deficits of synaptic transmission and presynaptic function in 22q11DS mice

To rescue the disruption of TC synaptic transmission in *Df(16)1/+* mice, we replenished miR-338-3p in the thalamic-relay neurons by injecting *AAV-GFP-miR-338-3p* into the MGv in vivo using an approach similar to that used in previous experiments (Fig. 2h); *AAV-GFP* was used as a control (Fig. 3a). Three to 4 weeks later, AAV infection yielded a robust expression of GFP in the MGv neurons, and the GFP-labeled projections were clearly visible in the L3/4 thalamorecipient layer of the ACx (Fig. 3b). We recorded the input–output relations at TC projections in 4- to 5-month-old WT and *Df(16)1/+* mice injected with either *AAV-GFP-miR-338-3p* or *AAV-GFP.* As in previous experiments[5] (Fig. 1d), we observed a substantial deficit in TC synaptic transmission between WT and *Df(16)/1+* mice injected with *AAV-GFP*. WT mice injected with *AAV-GFP-miR-338-3p* did not show a

significant increase in synaptic transmission compared to controls. However, the TC synaptic transmission deficit was rescued in *Df(16)1/+* mice injected with *AAV-GFP-miR-338-3p* (Fig. 3c). Similarly, the presynaptic TC deficit observed in *Df(16)1/+* mice[5] was rescued by replenishing miR-338-3p. Injections of *AAV-GFP-miR-338-3p* but not *AAV-GFP* into the MGv rescued a deficient paired-pulse ratio (PPR) of two consecutive TC EPSCs in *Df(16)1/+* mice without affecting TC PPR in WT mice at all measured interpulse intervals (Fig. 3d). These results indicate that depletion of miR-338-3p is a necessary component for developing TC deficits in 22q11DS mouse models.

miR-338 depletion in the MGv or *miR-338*–knockout recapitulates the auditory TC synaptic abnormalities of 22q11DS mice

To test whether miR-338-3p depletion is sufficient to trigger TC deficits, we employed two strategies. First, we constructed an miR-338-3p sponge by using a previously described strategy[40]. Second, we generated *miR-338*–knockout (KO) mice (Fig. 4d). The miR-338-3p sponge efficiency was verified in an in vitro system by using the luciferase assay. The sponge with 12 seed sites substantially and specifically depleted miR-338-3p levels in vitro (Fig. S3). On the basis of these data, we constructed AAVs expressing either the miR-338-3p sponge or a scrambled control vector under the control of the *CamKIIα* promoter (Fig. 4a). An AAV expressing the miR-338-3p sponge injected into the MGv of WT mice was sufficient to increase *Drd2* mRNA (Fig. 4b) and render the TC projections sensitive to haloperidol (Fig. 4c).

We then generated a mutant mouse lacking *miR-338* (*miR-338* KO mice) (Fig. 4d). The locus of *miR-338* is within the seventh intron of the apoptosis-associated tyrosine kinase (*Aatk*) gene. However, unlike miR-338-3p, *Aatk* expression in the MGv was not affected by age or *miR-338* deletion (Fig. S4a,b). The *miR-338* KO mice lacked miR-338-3p, miR-338-5p, and miR-3065 (both -3p and -5p species), whose genomic loci overlap with that of *miR-338*. However, miR-338-5p, miR-3065-3p, and miR-3065-5p were not *Drd2*-targeting miRNAs, as predicted by the microRNA target–prediction algorithms, and their expression levels in the auditory thalamus were 0% to 2.5% that of miR-338-3p (Fig. S4c). The *miR-338*$^{+/-}$ or *miR-338*$^{-/-}$ mice developed normally (Fig. S4d,e). Their *Drd2* RNA levels were inversely correlated with miR-338-3p levels in the auditory thalamus (Fig. 4e). Moreover, Drd2 protein levels were elevated in the MGv but not in the cortex or hippocampus of *miR-338*$^{+/-}$ or *miR-338*$^{-/-}$ mice (Fig. 4f), further indicating that miR-338-3p regulates *Drd2* expression in the auditory thalamus.

Because miR-338-3p is depleted but not eliminated in *Df(16)1/+* mice, we tested TC synaptic properties in 4-month-old *miR-338*$^{+/-}$ mice. Like that in *Df(16)1/+* mice[5], synaptic transmission at TC projections was substantially disrupted in *miR-338*$^{+/-}$ mice. The input–output function, which we tested by electrical stimulation of TC projections, showed a decrease in TC EPSCs in *miR-338*$^{+/-}$ mice compared to that in WT mice (Fig. 4g,h). This disruption was specific to TC projections. The input–output function tested by electrical stimulation of corticocortical (CC) projections in the same slices did not differ between *miR-338*$^{+/-}$ and WT mice (Fig. 4i). The PPR of two consecutive electrically evoked EPSCs was substantially altered in TC but not CC projections of *miR-338*$^{+/-}$ mice compared to that

in WT controls (Fig. 4j,k). In contrast, the NMDAR/AMPAR ratio (a measure of the postsynaptic function) was normal in both TC and CC projections of *miR-338*$^{+/-}$ mice (Fig. 4l,m). Because electrical stimulation of the thalamic radiation may affect circuits other than TC projections[41], we activated TC projections more selectively using the optogenetic approach. To that end, we injected AAVs expressing ChR2 under the control of *CamKIIα* into the MGv of *miR-338*$^{+/-}$ and WT littermates. We then activated TC projections by using 473-nm light pulses (Fig. 4n). The input–output relations and PPR (but not the NMDAR/AMPAR ratio) of optically evoked EPSCs were substantially decreased in 4-month-old *miR-338*$^{+/-}$ mice compared to that in WT littermates (Fig. 4o–q), which recapitulated the TC disruption in 22q11DS mouse models.

miR-338 haploinsufficiency disrupts TC transmission by decreasing the release probability of thalamic projections

We previously showed that the TC disruption of synaptic plasticity in 22q11DS mouse models was due to defective presynaptic function, which was in turn was caused by reduced probability of glutamate release from thalamic projections[5]. Abnormalities in the input–output relation and PPR at TC projections of *miR-338*$^{+/-}$ mice also suggested a deficit in presynaptic function at TC glutamatergic synapses. To understand the nature of this deficit, we performed two-photon calcium imaging in dendritic spines, which are the inputs of thalamic projections onto thalamorecipient neurons in the ACx. We loaded L3/4 pyramidal neurons with the calcium indicator Fluo-5F and cytoplasmic dye Alexa 594 (Fig. 5a) and identified dendritic spines that responded to electrical stimulation of the thalamic radiation (Fig. 5b). This method enabled us to measure three factors that may contribute to the TC disruption: the distribution of synaptic inputs on dendritic trees of postsynaptic neurons, the amplitudes of calcium transients, and the probability of calcium transients at individual dendritic spines (a proxy for the probability of neurotransmitter release measured at a single synaptic input)[42, 43]. The distribution of active TC inputs on dendritic trees and the peak amplitudes of postsynaptic calcium transients in *miR-338*$^{+/-}$ mice were comparable to that in WT mice (Fig. 5c–e), suggesting that TC development, pathfinding, synaptic targeting of cortical neurons by TC projections, and postsynaptic glutamatergic receptor function were not compromised in *miR-338*$^{+/-}$ mice. Note that although this negative result shows the lack of a deficit in TC morphology, it does not rule out potential morphological deficits on a finer subsynaptic scale. Interestingly, the probability of calcium transients in dendritic spines of thalamorecipient neurons in response to a low-frequency (0.1 Hz) train of stimuli was deficient in *miR-338*$^{+/-}$ mice (Fig. 5f). This result indicates that the depletion of miR-338 decreased the probability of glutamate release at TC projections, which underlies the TC disruption in 22q11DS. This deficit in the probability of glutamate release was rescued in slices treated with haloperidol (Fig. 5f). Haloperidol also effectively rescued the deficit in the probability of glutamate release in the same dendritic spine. The probability of detecting the calcium transient increased in *miR-338*$^{+/-}$ (but not WT) dendritic spines after haloperidol application (Fig. 5g,h). This finding further demonstrates that haloperidol rescues the presynaptic deficit of TC synaptic transmission in *miR-338* KO mice.

miR-338 depletion eliminates the age dependency of TC disruption and PPI

The deletion of *miR-338* was sufficient to upregulate *Drd2* in the thalamus, which suggested that depletion of only this miRNA underlies the abnormal sensitivity of TC projections in 22q11DS to antipsychotics. To test this hypothesis, we compared the sensitivity of TC projections in *miR-338*$^{+/-}$ mice and WT mice. First, we determined that TC projections of *miR-338*$^{+/-}$ (but not WT) mice were sensitive to the Drd2-specific antagonist L-741,626 (20 nM) (Fig. 6a). In *miR-338*$^{+/-}$ mice, TC EPSCs substantially increased in response to L-741,626, but that increase was not further elevated by haloperidol. Haloperidol alone increased TC EPSCs in 4-month-old *miR-338*$^{+/-}$ mice (but not in WT mice) to magnitudes similar to those observed in *Df(16)1/+* or *Dgcr8*$^{+/-}$ mice, suggesting that haloperidol's effect in mutant TC projections was mediated by elevated expression of Drd2 receptors (Figs. 6b, S5). Similarly, other antipsychotics (i.e., clozapine and olanzapine) increased TC EPSCs to similar magnitudes in *miR-338*$^{+/-}$ mice but not WT mice (Fig. S6).

Unlike *Df(16)1/+* or *Dgcr8*$^{+/-}$ mice, *miR-338*$^{+/-}$ mice became sensitive to haloperidol in an age-independent manner (Figs. 6b, S5). Furthermore, in young (2-month-old) WT mice, TC projections became sensitive to haloperidol when the miR-338-3p sponge was expressed in the MGv (Fig. S7), indicating that depletion of miR-338-3p in the MGv is sufficient for sensitivity to antipsychotics. TC sensitivity to haloperidol in 2-month-old *miR-338*$^{+/-}$ mice was eliminated by expression of small inhibitory RNA (siRNA) against *Drd2* (but not a control siRNA) in the MGv (Fig. 6c,d). The specificity of Drd2 siRNA has been characterized previously[5]. These experiments further indicate that miR-338-3p is sufficient to regulate Drd2 in the thalamus, regardless of age. Similarly, *miR-338*$^{+/-}$ mice were deficient in PPI compared to that in WT controls, and this deficit was observed at all tested time points (1.5, 2, and 4 months) (Fig. 6e–g). The defect in PPI was not caused by peripheral hearing defects because the acoustic brainstem-response testing showed no differences between *miR-338*$^{+/-}$ and WT mice at these ages (Fig. S8).

Discussion

The recent identification of disrupted glutamatergic synaptic transmission at thalamic inputs to the ACx in 22q11DS mice[5] suggests that TC disruption could be a pathogenic mechanism that mediates the susceptibility to positive psychotic symptoms in 22q11DS-related schizophrenia for the following reasons: 1) TC disruption in 22q11DS mice is rescued by antipsychotic medications that are Drd2 antagonists and effectively treat predominantly psychotic symptoms but not cognitive or negative symptoms of schizophrenia[44–46]. This disruption was specific to auditory TC projections and not observed at other glutamatergic projections (i.e., hippocampal, corticocortical, or corticofugal projections) that may be involved in cognitive, social, or motivational tasks. 2) TC disruption in 22q11DS mice is caused by abnormal elevation of *Drd2* mRNA and Drd2 protein levels in the TC neurons in the thalamus, a brain region previously linked to psychotic symptoms of schizophrenia[47, 48]. The increase in dopamine signaling in the thalamus was also described in schizophrenic patients[49], and studies have indicated that drug-naïve schizophrenic patients have elevated levels of DRD2s in other brain regions[50, 51]. Furthermore, theoretical and empirical studies have proposed that deficient connectivity and abnormal patterns of activity in TC projections

contribute to the pathogenesis of the disease[52–55]. Moreover, a local ischemic infarction that disrupts auditory TC projections in a nonpsychotic patient can cause auditory hallucinations[56]. 3) Sensitivity to antipsychotics is observed in the auditory but not the visual or somatosensory TC projections of 22q11DS mice, which is consistent with clinical observations of the substantially higher prevalence of auditory hallucinations, compared with that of hallucinations in other sensory modalities, in schizophrenia[28]. Neuroimaging and electrophysiological studies in schizophrenia patients have shown abnormal activation of the auditory thalamus and ACx during auditory hallucinations[1, 3, 21]. 4) Drd2 elevation only in the auditory thalamus of 22q11DS mice was sufficient to reduce the PPI of the acoustic startle response[5], the behavioral endophenotype characteristic of patients with one of several psychiatric diseases, including 22q11DS and schizophrenia[38, 57].

Here we showed that the disruption of synaptic transmission at auditory TC projections recapitulates another prominent feature of psychotic symptoms. The TC disruption in 22q11DS mice becomes evident only after 3 months of age, which is equivalent to the age of approximately 20 years in humans[35]. These data correspond well with the onset of clinical manifestations of psychosis in patients with 22q11DS (median age, 21 years[25]) or schizophrenia during late adolescence or early adulthood, typically between the ages of 16 and 30 years[26, 58]. This age-dependent TC decrease in synaptic function is evident in *Df(16)1/+* mice, which carry a large microdeletion, and in *Dgcr8*$^{+/-}$ mice, further strengthening the case that *Dgcr8* is the culprit gene, and its haploinsufficiency underlies auditory abnormalities in 22q11DS.

Previous work established that the deletion of one copy of *Dgcr8* leads to the elevation of Drd2 in the auditory thalamus[5]. Because Dgcr8 is part of the miRNA-processing machinery, we hypothesized that a *Dgcr8–miRNA–Drd2* mechanism underlies the disruption of TC synaptic transmission. Here we identified miR-338-3p as the mediator of this mechanism (Fig. 6h). We also showed that miR-338-3p negatively regulates the level of *Drd2* in the thalamus. Replenishing miR-338-3p in the thalamus eliminates deficient TC synaptic transmission and abnormal antipsychotic sensitivity of TC projections in 22q11DS mice, and the deletion or auditory thalamus–specific knockdown of miR-338-3p mimics TC disruption of synaptic transmission and antipsychotic sensitivity in WT mice. Depletion of miR-338-3p is therefore necessary and sufficient to upregulate Drd2 in the thalamus, which in turn, reduces glutamate release from thalamic projections, reduces TC synaptic transmission, and renders TC projections sensitive to antipsychotics (Fig. 6h). Because miR-338-3p is enriched in the auditory thalamus and more abundant miRNAs more effectively regulate the targeting transcripts[39], miR-338-3p reduction in the thalamus (but not in tissues where it is weakly expressed) would upregulate Drd2 and provide tissue specificity.

TC disruption in 22q11DS mice and *miR-338*-deficient mice correlates with deficits in PPI, an impaired sensorimotor gating feature that occurs in schizophrenia and several other neuropsychiatric disorders. The importance of the auditory thalamus for PPI is well known[59], but the effect of disrupting TC projections on PPI deficits is not. Therefore, other projections emanating from the auditory thalamus and containing depleted miR-338-3p and upregulated Drd2 might cause PPI deficits in 22q11DS mice.

One copy of *Dgcr8* is deleted in 22q11DS, in all cells at all ages, so it is unclear why synaptic disruption occurs in projections emanating only from the thalamus and only later in life. The regional specificity most likely arises from the fact that miR-338-3p is substantially enriched in the auditory thalamus compared to other brain regions, such as the cortex or hippocampus. Explaining why miR-338-3p is thalamus-enriched will require further investigation. We also determined that the expression of miR-338-3p is regulated in an age-dependent manner. Although miR-338-3p is depleted in the auditory thalamus in 22q11DS mice at all ages, compared to WT mice, it declines further with age in both 22q11DS and WT mice. Therefore, miR-338-3p expression may be controlled by a combination of *Dgcr8*- and age-dependent mechanisms. Although we can assume that *Dgcr8* haploinsufficiency reduced the levels of miRNAs, the mechanism of age-dependent miRNA decline is unknown. In the context of Drd2 regulation, a minimal threshold of miR-338-3p expression probably triggers the overexpression of Drd2. In WT mice, miR-338-3p declines during the first few months of life, but it may not reach that threshold. However, in 22q11DS mice, *Dgcr8* haploinsufficiency and age-dependent decline in miRNA production drives the miR-338-3p level below this threshold, triggers the elevation of Drd2 in the thalamus, and causes TC synaptic and behavioral deficiencies.

In summary, our data implicate thalamus-enriched miR-338-3p as the key mediator of disruption of synaptic transmission at TC projections and late onset of auditory symptoms of 22q11DS. Our data also suggest that replenishment of miR-338-3p in the thalamus could be a more tolerable therapeutic approach for positive symptoms. Current therapy relies upon antipsychotics to alleviate psychosis in schizophrenic patients through systemic inhibition of DRD2, which is accompanied by multiple, and sometimes devastating, side effects[27, 60]. Given that the seed sites of miR-338-3p are conserved between humans and mice, miR-338-3p is enriched in the thalamus of both species and becomes depleted in the thalamus of mouse models of 22q11DS and schizophrenic patients, this strategy is potentially applicable to patients. Thus, our results suggest that miR-338-3p is a potential therapeutic target for treating positive symptoms of 22q11DS and related cases of schizophrenia.

Online Methods

Animals

Mice of both sexes were used for all experiments. *Df(16)1/+* and *Dgcr8*$^{+/-}$ mouse strains were reported previously[6, 31] and were back-crossed onto the C57BL/6J genetic background for at least 10 generations. Mice ranging in age from 1.5 to 7 months were used, which approximately corresponds to 13 to 35 years in humans[35] (https://www.jax.org/research-and-faculty/research-labs/the-harrison-lab/gerontology/life-span-as-a-biomarker). The *miR-338*$^{+/-}$ and *miR-338*$^{-/-}$ mice were generated from embryonic stem cells from C57BL/6N-A^{tm1Brd} mice that were purchased from the Mutant Mouse Regional Resource Center (MMRRC; clone #034476-UCD). These cells were tested and found negative for mycoplasma contamination. C57BL/6 blastocyst injections were performed by the Transgenic/Gene Knockout Shared Resource at St. Jude Children's Research Hospital (St. Jude). Chimeric mice were genotyped according to MMRRC protocols by using the

following primers: 5′ common reverse (ATAGCATACATTATACGAAGTTATCACTGG), 5′ gene-specific (CTTCACTACACTCTCCCTAGTACAGTCTC), 3′ common forward (TCTAGAAAGTATAGGAACTTCCATGGTC), and 3′ gene-specific (AGGAGACTCATAGTTCTCTGTATCATAGC). PCR was performed under the following conditions: 93 °C for 3 min, 93 °C for 15 s, and 68 °C for 9 min for 8 cycles and then 93 °C for 15 s, 60 °C for 30 s, and 68 °C for 9 min for 32 cycles. The mutant allele generated a 6.1-kb band with 5′ common-reverse and 5′ gene-specific primers and a 4.1-kb band with 3′ common-forward and 3′ gene-specific primers. The wild-type (WT) allele did not generate a band with either primer set. Subsequent genotyping was performed at Transnetyx (Cordova, TN). For the majority of experiments, mice were divided into groups according to genotype or viral injections, and the experimenters were blinded to the genotype or treatment. The care and use of animals were reviewed and approved by the St. Jude Institutional Animal Care and Use Committee.

Whole-Cell Electrophysiology

Acute primary thalamocortical (TC) slices (400-μm thick) containing the left auditory cortex (ACx) and the left ventral part of the medial geniculate nuclei (MGv) of the thalamus were prepared as previously described[5, 61]. Briefly, mouse brains were quickly removed and placed in cold (4 °C) dissecting artificial cerebrospinal fluid (ACSF) containing 125 mM choline-Cl, 2.5 mM KCl, 0.4 mM $CaCl_2$, 6 mM $MgCl_2$, 1.25 mM NaH_2PO_4, 26 mM $NaHCO_3$, and 20 mM glucose (300–310 mOsm), with 95% O_2/5% CO_2. Primary TC slices were obtained from the left hemisphere by using a slicing angle of 15°. After a 1-h incubation in ACSF [125 mM NaCl, 2.5 mM KCl, 2 mM $CaCl_2$, 2 mM $MgCl_2$, 1.25 mM NaH_2PO_4, 26 mM $NaHCO_3$, 20 mM glucose (300–310 mOsm), with 95% O_2/5% CO_2] at room temperature, the slices were transferred into the recording chamber and superfused (2–3 mL/min) with warm (30–32 °C) ACSF.

Whole-cell recordings were obtained from cell bodies of layer (L) 3/4 thalamorecipient neurons in the ACx and thalamic-relay neurons in the MGv. Mice were chosen in a pseudorandom order, without the experimenter's prior knowledge of genotype or treatments. Patch pipettes (open-pipette resistance, 3.5–5 MΩ) were filled with an internal solution containing 125 mM $CsMeSO_3$, 2 mM CsCl, 10 mM HEPES, 0.1 mM EGTA, 4 mM MgATP, 0.3 mM NaGTP, 10 mM Na_2 creatine phosphate, 5 mM QX-314, 5 mM tetraethylammonium Cl (pH 7.4 adjusted with CsOH, 290–295 mOsm). Voltage-clamp recordings were made using a Multiclamp 700B, digitized (10 kHz), and recorded using the pCLAMP 10.0 software. Excitatory postsynaptic currents (EPSCs) were recorded at holding membrane potentials of –70 mV. In all experiments, membrane potentials were corrected for a liquid junction potential of –10 mV. TC EPSCs were evoked by current pulses (duration, 100 μs) delivered to the thalamic radiation via tungsten bipolar electrodes. The stimulation intensities were similar in experiments in Fig. 1f–g (2 months: 527 ± 61 μA, 19 neurons in WT and 568 ± 50 μA, 21 neurons in *Df(16)/+* mice; $p > 0.05$; 4 months: 523 ± 42 μA, 31 neurons in WT and 550 ± 39 μA, 30 neurons in *Df(16)/+* mice; $p > 0.05$) and Fig. 1i–j (2 months: 569 ± 44 μA, 16 neurons in WT and 582 ± 37 μA, 24 neurons in $Dgcr8^{+/-}$ mice; $p > 0.05$; 4 months: 543 ± 43 μA, 36 neurons in WT and 551 ± 43 μA, 37 neurons in $Dgcr8^{+/-}$ mice; $p > 0.05$).

Paired-pulse ratio (PPR) of TC and corticocortical (CC) EPSCs and the NMDAR/AMPAR ratio were measured as described previously[5]. The first 2 ms of the EPSC slope were measured as an accurate indicator of monosynaptic strength at TC synapses[62]. Changes in the EPSC slope correlated with changes in the EPSC amplitude and EPSC charge[5]. To ensure consistent access resistance of the recording electrode during long-term experiments, we monitored the peak amplitude of a brief (10-ms) hyperpolarizing test pulse (–5 mV), which was given 250 ms after a stimulus. Access resistance in recorded neurons was typically 10 to 25 MΩ. Recordings were discarded if the access resistance was higher than 25 MΩ, or if it changed more than 15% during the course of the whole-cell recording.

Two-Photon Imaging

Two-photon laser-scanning microscopy was performed using an Ultima imaging system, a Ti:sapphire Chameleon Ultra femtosecond-pulsed laser, and 60× (0.9 NA) water-immersion infrared objectives. Synaptically evoked calcium transients were measured in dendritic spines, the site of thalamic inputs, as described previously[43]. Briefly, Alexa Fluor 594 (30 μM) and Fluo-5F (300 μM) were included in the internal pipette solution (see above) and were excited at 820 nm. Synaptically evoked changes in fluorescence of both fluorophores were measured in the line-scan mode (750 Hz) in spine heads and the parent dendritic shaft. Line scans were analyzed as changes in green (G, Fluo-5F) fluorescence normalized to red (R, Alexa Fluor 594) fluorescence ($\Delta G/R$). The amplitude and probability of calcium transients were measured in response to 10 to 20 stimulations delivered at 0.1 Hz to the thalamic radiation. Distance (angular) of the active thalamic inputs from the center of the soma was calculated using maximum-intensity projections of z-scan images of the entire cell collected at lower magnification.

Optogenetics

In optogenetic experiments, we expressed the light-activated cation channel ChR2 in the MGv by using adeno-associated virus (AAV) and evoked optically induced EPSCs by briefly illuminating TC slices with a 473-nm light[63]. AAVs were generated from the pAAV-CaMKIIα-hChR2(H134R)-YFP-WPRE-pA (CamKIIα-ChR2-YFP) plasmid and produced commercially (UNC Vector; serotype 2/1; 4×10^{12} IFU/mL). AAVs were injected into the MGv as described previously[41]. Adult mice were anesthetized with isoflurane in pure oxygen, and a 200- to 400-nL sample of virus was slowly pressure-injected into the MGv (from the bregma: anterior-posterior, –3.0 mm; medial-lateral, ± 2.0 mm; dorsal-ventral, 3.1 mm). Approximately 21 to 28 days after virus injection, the mice were decapitated, and TC slices were prepared. Confocal imaging of YFP in the MGv was used to verify on-target infection of CamKIIα-ChR2-YFP viruses. Short light pulses (10–200 mW) from a 473-nm laser were directed to the slices through the visible light photoactivation module or through the objective.

miRNA Microarray

Total RNA was isolated from 2- and 4-month-old male WT, *Df(16)1/+*, and *Dgcr8*$^{+/-}$ thalami containing MGv by using the mirVana RNA isolation kit (Life Technologies, Carlsbad, CA). Total RNAs (100 ng) were labeled using miRNA Complete Labeling and Hyb Kit (Agilent, Santa Clara, CA), followed by hybridizing to the Mouse miRNA v19

Microarray (Agilent-046065) that contains 3105 unique probes targeting 1247 mature miRNAs, according to the mouse miRBase version 19.0 (www.mirbase.org; August 2012). Microarrays were scanned using an Agilent array scanner (G2565CA) at 3-μm resolution. Microarray data were extracted by Agilent Feature Extraction software (v.10.5.1.1) using the miRNA_107_Sep09 protocol. The data process was performed using Partek software (St. Louis, MO).

After quantile normalization among arrays, each probe was summarized by averaging intensities with a single normalized intensity value. The Student's *t*-test was used to determine statistical significance between sets of replicates from different experimental groups. The miRNA was considered significantly differentially expressed when the p-value was less than 0.01 for more than one probe targeting the mature form of the miRNA. The mRNAs targeted by differentially expressed miRNAs were predicted using bioinformatics tools miRWalk[64] and TargetScan (www.targetscan.org).

Quantitative RT-PCR

Total RNA was isolated from various brain regions (i.e., the auditory thalamus containing the MGv, hippocampus, or cortex) or from SH-SY5Y cells (ATCC, CRL-2266) by using the mirVana RNA Isolation Kit (Life Technologies). The iScript kit (Bio-Rad, Hercules, CA) was used to synthesize cDNA from mRNA, and the miRNA First-Strand cDNA Synthesis Kit (Agilent) was used to synthesize cDNA from miRNA. The experiments were performed using SYBR Green (Life Technologies). The following forward primers were used for miRNA analysis: mmu-miR-338-3p and hsa-miR-338-3p (TCCAGCATCAGTGATTTTGTTG), mmu-miR-335-3p (TTTTTCATTATTGCTCCTGACC), mmu-miR-335-5p (TCAAGAGCAATAACGAAAAATGT), mmu-miR-337-3p (TCAGCTCCTATATGATGCCTTT), mmu-miR-337-5p (CGGCGTCATGCAGGAGTTGATT), mmu-miR-3065-5p (TCAACAAAATCACTGATGCTGG), and mmu-miR-3065-3p (TCAGCACCAGGATATTGTTGGGG). The universal reverse-primer specific to the sequence tag (miRNA First-Strand cDNA Synthesis Kit) was used. The following primers were used for mRNA analysis: *Drd2* forward (GGATGTCATGATGTGCACAGC), *Drd2* reverse (CGCTTGCGGAGAACGATG), *Aatk* forward (ATGCTGGCCTGCCTGTGTTGT), and *Aatk* reverse (AGGGGCAGGACATACACATCGG). The following loading controls were used: *U6 snRNA* forward (CGCTTCGGCAGCACATATAC), *U6 snRNA* reverse (TTCACGAATTTGCGTGTCAT) (the same primers were used for mouse and human samples), SnoRNA202 (CTTTTGAACCCTTTTCCATCTG), and SnoRNA234 (TTAACAAAAATTCGTCACTACCA). The same universal reverse primer was used for SnoRNA202 and SnoRNA234. To measure *DRD2* mRNA in SH-SY5Y cells, the Lipofectamine 2000 (Invitrogen) method was used to transfect these cells with pGIPZ plasmids (Open Biosystems) containing an miRNA of interest or an empty vector (control). The following primers were used to clone hsa-miR-337-3p and hsa-miR-337-5p into the pGIPZ plasmid: hsa-miR-337-3p-1 (TCGAGGCTGTTGACAGTGAGCGACCTCCTATATGATGCCTTTCTTCTGTGAA); hsa-miR-337-3p-2,

(CCATCTGTGGCTTCACGAAGAAAGGCATCATATAGGAGGTCGCTCACTGTCAACAGCC); hsa-miR-337-3p-3 (GCCACAGATGGGAAGAAAGGCATCATATAGGAGGCTGCCTACTGCCTCGGAA); hsa-miR-337-3p-4 (TCGATTCCGAGGCAGTAGGCAGC CTCCTATATGATGCCTTTCTTC); hsa-miR-337-5p-1, (TCGAGGCTGTTGACAGTGAGCGACGAACGGCTTCATACAGGAGTTTGTGAA); hsa-miR-337-5p-2, (CCATCTGTGGCTTCACAACTCCTGTATGAAGCCGTTCGTCGCTCACTGTCAACAGCC); hsa-miR-337-5p-3 (GCCACAGATGGAACTCCTGTATGAAGCCGTTCGCTGCCTACTGCCTCGGAA); hsa-miR-337-5p-4, (GCCACAGATGGAACTCCTGTATGAAGCCGTTCGCTGCCTACTGCCTCGGAA). For cloning hsa-miR-335-3p, hsa-miR-335-5p, and hsa-miR-338-3p (all three are conserved between mice and humans), the primers given below were used. The following primers were used in SH-SY5Y cells: *DRD2* forward (GAGTGGAAATTCAGCAGGATTC); *DRD2* reverse (GAAGGACAGGACCCAGACGATG); *turboGFP* forward (CTTCAGCTACCGCTACGAGG); and *turboGFP* reverse (GCTCTTGAAGTGCATGTGGC). *DRD2* levels were normalized to *turboGFP*. Samples from each mouse or each well containing SH-SY5Y cells were run in triplicate.

Western blotting

Mouse brain tissues were lysed in ice-cold RIPA buffer (50 mM Tris-HCl [pH 7.4], 1% NP-40, 0.25% sodium deoxycholate, 150 mM NaCl, and 1 mM EDTA) that included protease inhibitor cocktail tablets. A total of 25 μg (MGv) or 30 μg (cortex, hippocampus) protein was loaded per lane. Sodium dodecyl sulfate/polyacrylamide gel electrophoresis, protein transfer to polyvinylidene difluoride membranes, and Western blotting were performed using standard techniques. The following primary antibodies were used: rabbit anti-DRD2 (Abcam, ab85367; 1:500) and mouse anti– β-actin (Sigma-Aldrich, A5316, 1:10,000). The following secondary antibodies were used: anti-rabbit (LI-COR Biosciences, 926-68021; 1:15000) and anti-mouse (LI-COR Biosciences, 926-32212, 1:15000) antibodies conjugated to IR dye 680 or 800, respectively. Blots were imaged and quantified using the Odyssey CLx infrared imaging system. Samples from each mouse were run in triplicate.

Human brain tissue

Postmortem samples of human MGv and ACx (Brodmann area 41) were obtained from The Maryland Brain Collection (Maryland Psychiatric Research Center, University of Maryland School of Medicine, Catonsville, MD). We tested the level of mature miR-338-3p in patients with schizophrenia and age-, race-, and sex-matched healthy controls. Only samples with RNA integrity number higher than 7 were used in these experiments (Agilent RNA 6000 Nano kit). The mean postmortem interval was 15.3 ± 2.0 h for patients with schizophrenia and 17.2 ± 1.6 h ($p>0.05$) for healthy controls. Quantitative RT-PCR for each brain tissue sample was run in triplicate.

Plasmids and Viruses

To overexpress the miRNAs of interest, we generated recombinant AAVs (serotype 5) by cloning chimeric hairpins of the miRNAs of interest with hsa-miR-30a into the 3′UTR of *GFP* under the control of the *CamKIIα* promoter by using a previously described strategy[65]. The following primers were used: miR-338-3p-1 (GTACAGCTGTTGACAGTGAGCGACTCCAGCATCAGTGATTTTGTTGTGTGAA), miR-338-3p-2 (CCATCTGTGGCTTCACACAACAAAATCACTGATGCTGGAGTCGCTCACTGTCAACAGCT), miR-338-3p-3 (GCCACAGATGGCAACAAAATCTGATGCTGGAGCTGCCTACTGCCTCGGAA), miR-338-3p-4 (AGCTTTCCGAGGCAGTAGGCAGCTCCAGCATCAGATTTTGTTG), miR-337-3p-1 (GTACAGCTGTTGACAGTGAGCGACTCAGCTCCTATATGATGCCTTTTGTGAA), miR-337-3p-2 (CCATCTGTGGCTTCACAAAAGGCATCATATAGGAGCTGAGTCGCTCACTGTCAACAGCT), miR-337-3p-3 (GCCACAGATGGAAAGGCATCATAGGAGCTGAGCTGCCTACTGCCTCGGAA), miR-337-3p-4 (AGCTTTCCGAGGCAGTAGGCAGCTCAGCTCCTATGATGCCTTT), miR-337-5p-1 (GTACAGCTGTTGACAGTGAGCGACCGGCGTCATGCAGGAGTTGATTTGTGAA), miR-337-5p-2 (CCATCTGTGGCTTCACAAATCAACTCCTGCATGACGCCGGTCGCTCACTGTCAACAGCT), miR-337-5p-3 (GCCACAGATGGAATCAACTCGCATGACGCCGGCTGCCTACTGCCTCGGAA), miR-337-5p-4 (AGCTTTCCGAGGCAGTAGGCAGCCGGCGTCATGCGAGTTGATT), miR-335-3p-1 (GTACAGCTGTTGACAGTGAGCGACTTTTTCATTATTGCTCCTGACCTGTGAA), miR-335-3p-2 (CCATCTGTGGCTTCACAGGTCAGGAGCAATAATGAAAAAGTCGCTCACTGTCAACAGCT), miR-335-3p-3 (GCCACAGATGGGGTCAGGAGATAATGAAAAAGCTGCCTACTGCCTCGGAA), miR-335-3p-4 (AGCTTTCCGAGGCAGTAGGCAGCTTTTTCATTATCTCCTGACC), miR-335-5p-1 (GTACAGCTGTTGACAGTGAGCGACTCAAGAGCAATAACGAAAAATGTTGTGAA), miR-335-5p-2 (CCATCTGTGGCTTCACAACATTTTTCGTTATTGCTCTTGAGTCGCTCACTGTCAACAGCT), miR-335-5p-3 (GCCACAGATGGACATTTTTCGATTGCTCTTGAGCTGCCTACTGCCTCGGAA), and miR-335-5p-4 (AGCTTTCCGAGGCAGTAGGCAGCTCAAGAGCAATCGAAAAATGT).

The miR-338-3p sponges were generated as described previously[66, 67]. Twelve copies of the following sequences were inserted for the miR-338-3p sponge (CAACAAAATGCGGATGCTGGA) or scrambled control (GACACTGTGAGCGAAGACATA) into the 3′UTR of *GFP* under the control of the *CamKIIα* promoter. Recombinant AAVs (1-2 × $10^{13–14}$ particles/mL) were generated at the

St. Jude Vector Development & Production Core and injected into the MGvs of anesthetized mice, as described previously[5].

In the luciferase assay, multiple copies of the miR-338-3p sponge and scramble control were cloned into 3′-UTR of Renilla luciferase gene contained within the psiCHECK-2 vector (Promega). To test the effect of the sponge in cells, the plasmids were transfected into HEK 293T (ATCC, CCL-3216) or Neuro 2a (ATCC, CCL-131) cells along with control pcDNA3.1 or primary miR-338, miR-337, miR-335, and irrelevant miR-185–overexpressing plasmids. The cell lines were not authenticated or tested for mycoplasma. After 2 days in culture, Renilla and Firefly activities were measured using the dual-luciferase reporter assay (Promega) according to the manufacturer's instructions. The Renilla luciferase expression was normalized to Firefly luciferase expression as a readout.

Mouse Behavioral Tests

Prepulse inhibition (PPI) experiments were performed as previously described[5]. Briefly, each day before testing, the mice were transported from the animal-housing room and allowed a 1-h habituation period in the testing room. Before experiments were initiated, the mice had a 20-min acclimation period in the Plexiglas restraint chamber (6 cm × 6 cm × 4.8 cm). The mice then had a 5-min acclimation period to 65-dB background white noise, which played throughout the session. For PPI experiments, 3 acoustic startles [white noise (1–20 kHz), 120 dB, 40 ms] were delivered, separated by a 15-s intertrial interval. The testing session consisted of the following trials: pulse-alone, in which the startle pulse was presented; the combination of a 40-ms white-noise prepulse (74 dB, 82 dB, or 90 dB) in WT and *Dgcr8*$^{+/-}$ littermates and (70 dB, 80 dB, or 90 dB) in WT and *miR-338*$^{+/-}$ littermates and preceding the startle pulse by 100 ms, and no stimuli. Trials were separated by 15 s and presented in a pseudo-random order. PPI was calculated as follows: 100 × (pulse-alone response – prepulse + pulse response)/pulse-alone response.

Auditory brainstem response (ABR) experiments were performed as previously described[68]. Briefly, mice were anesthetized with Avertin (0.6 mg/g bodyweight, i.p.), and ABR was measured using a Tucker Davis Technology (TDT) System III with RZ6 Multiprocessor and BioSigRZ software. Sounds were delivered via the MF-1 speaker in the open-field configuration. ABR waveforms were recorded using subdermal needles placed at the vertex of the skull, below the pinna of the ear, and at the base of the tail. The needles were connected to a low-impedance headstage (RA4LI, TDT) and fed into the RZ6 multiprocessor through a preamplifier (RA4PA, Gain 20×, TDT). ABR waveforms were averaged from 500 presentations of a tone (21 tones/s) in the alternating phase and were band-pass filtered (300 Hz-3 kHz). The ABR threshold was defined as the minimum sound intensity that elicited a wave above the noise level. All ABR experiments were conducted in a sound booth (Industrial Acoustic Company, IAC, Model 120A double wall).

Statistical Analyses

All statistical data were computed using the Sigma Plot 12.5 software. Parametric or nonparametric tests were chosen based on the normality and variance of data distribution. Independent or paired two-tailed *t*-tests, Mann–Whitney rank-sum *U* test, one-way analysis

of variance (ANOVA)/Kruskal–Wallis one-way analysis of variance on ranks *H* test followed by a multiple comparison procedure (Dunn's method), two-way ANOVA/two-way repeated measures ANOVA with one factor repetition followed by Holm–Sidak multiple comparison procedure were the statistical tests used. *F*-values were reported for ANOVA. Differences with $p < 0.05$ were considered significant.

Data Availability

The microarray data are available in the NCBI GEO database under accession number GSE73981. miR-338 knockout mice are available upon request.

Supplementary Material

Refer to Web version on PubMed Central for supplementary material.

Acknowledgments

This work was supported by the National Institutes of Health grants MH097742, DC012833, and MH095810; the NARSAD Independent Investigator Award; and ALSAC (S.S.Z.). The funding sources had no role in the study design, data collection, data analysis, decision to publish, or preparation of the manuscript. We thank the St. Jude Vector Core for producing the AAVs, St. Jude Hartwell Center for Biotechnology & Bioinformatics for performing the microarrays, the Maryland Brain Collection for providing postmortem human brain samples, and Angela McArthur for editing the manuscript. The microRNA microarray data discussed in this publication have been deposited in NCBI's Gene Expression Omnibus and are accessible through GEO Series accession number GSE73981 http://www.ncbi.nlm.nih.gov/geo/query/acc.cgi?token=cpwxugcwdzsdhax&acc=GSE73981. Knockout mice, viruses, and other materials described in this manuscript can be obtained through a Material Transfer Agreement.

Reference List

1. Dierks T, et al. Activation of Heschl's gyrus during auditory hallucinations. Neuron. 1999; 22:615–621. [PubMed: 10197540]
2. Silbersweig DA, et al. A functional neuroanatomy of hallucinations in schizophrenia. Nature. 1995; 378:176–179. [PubMed: 7477318]
3. Horga G, Schatz KC, Abi-Dargham A, Peterson BS. Deficits in predictive coding underlie hallucinations in schizophrenia. J Neurosci. 2014; 34:8072–8082. [PubMed: 24920613]
4. Javitt DC, Sweet RA. Auditory dysfunction in schizophrenia: integrating clinical and basic features. Nat Rev Neurosci. 2015; 16:535–550. [PubMed: 26289573]
5. Chun S, et al. Specific disruption of thalamic inputs to the auditory cortex in schizophrenia models. Science. 2014; 344:1178–1182. [PubMed: 24904170]
6. Lindsay EA, et al. Congenital heart disease in mice deficient for the DiGeorge syndrome region. Nature. 1999; 401:379–383. [PubMed: 10517636]
7. Bassett AS, et al. Practical guidelines for managing patients with 22q11.2 deletion syndrome. J Pediatr. 2011; 159:332–339. [PubMed: 21570089]
8. McDonald-McGinn DM, Sullivan KE. Chromosome 22q11.2 deletion syndrome (DiGeorge syndrome/velocardiofacial syndrome). Medicine (Baltimore). 2011; 90:1–18. [PubMed: 21200182]
9. Scambler PJ, et al. Velo-cardio-facial syndrome associated with chromosome 22 deletions encompassing the DiGeorge locus. Lancet. 1992; 339:1138–1139. [PubMed: 1349369]
10. Karayiorgou M, Simon TJ, Gogos JA. 22q11.2 microdeletions: linking DNA structural variation to brain dysfunction and schizophrenia. Nat Rev Neurosci. 2010; 11:402–416. [PubMed: 20485365]
11. Pulver AE. Search for schizophrenia susceptibility genes. Biol Psychiatry. 2000; 47:221–230. [PubMed: 10682219]
12. Chow EW, Watson M, Young DA, Bassett AS. Neurocognitive profile in 22q11 deletion syndrome and schizophrenia. Schizophr Res. 2006; 87:270–278. [PubMed: 16753283]

13. Fung WL, et al. Elevated prevalence of generalized anxiety disorder in adults with 22q11.2 deletion syndrome. Am J Psychiatry. 2010; 167:998. [PubMed: 20693476]
14. Gothelf D, et al. Clinical characteristics of schizophrenia associated with velo-cardio-facial syndrome. Schizophr Res. 1999; 35:105–112. [PubMed: 9988847]
15. Green T, et al. Psychiatric disorders and intellectual functioning throughout development in velocardiofacial (22q11.2 deletion) syndrome. J Am Acad Child Adolesc Psychiatry. 2009; 48:1060–1068. [PubMed: 19797984]
16. Murphy KC, Jones LA, Owen MJ. High rates of schizophrenia in adults with velo-cardio-facial syndrome. Arch Gen Psychiatry. 1999; 56:940–945. [PubMed: 10530637]
17. Pulver AE, et al. Psychotic illness in patients diagnosed with velo-cardio-facial syndrome and their relatives. J Nerv Ment Dis. 1994; 182:476–478. [PubMed: 8040660]
18. Shprintzen RJ, Goldberg R, Golding-Kushner KJ, Marion RW. Late-onset psychosis in the velo-cardio-facial syndrome. Am J Med Genet. 1992; 42:141–142. [PubMed: 1308357]
19. Bassett AS, Chow EW, Weksberg R. Chromosomal abnormalities and schizophrenia. Am J Med Genet. 2000; 97:45–51. [PubMed: 10813803]
20. Murphy KC. Schizophrenia and velo-cardio-facial syndrome. Lancet. 2002; 359:426–430. [PubMed: 11844533]
21. Feinstein C, Eliez S, Blasey C, Reiss AL. Psychiatric disorders and behavioral problems in children with velocardiofacial syndrome: usefulness as phenotypic indicators of schizophrenia risk. Biol Psychiatry. 2002; 51:312–318. [PubMed: 11958782]
22. Bassett AS, et al. Clinical features of 78 adults with 22q11 Deletion Syndrome. Am J Med Genet A. 2005; 138:307–313. [PubMed: 16208694]
23. Vorstman JA, Breetvelt EJ, Thode KI, Chow EW, Bassett AS. Expression of autism spectrum and schizophrenia in patients with a 22q11.2 deletion. Schizophr Res. 2013; 143:55–59. [PubMed: 23153825]
24. Schneider M, et al. Psychiatric disorders from childhood to adulthood in 22q11.2 deletion syndrome: results from the International Consortium on Brain and Behavior in 22q11.2 Deletion Syndrome. Am J Psychiatry. 2014; 171:627–639. [PubMed: 24577245]
25. Bassett AS, et al. The schizophrenia phenotype in 22q11 deletion syndrome. Am J Psychiatry. 2003; 160:1580–1586. [PubMed: 12944331]
26. Mueser KT, McGurk SR. Schizophrenia. Lancet. 2004; 363:2063–2072. [PubMed: 15207959]
27. Lewis DA, Lieberman JA. Catching up on schizophrenia: natural history and neurobiology. Neuron. 2000; 28:325–334. [PubMed: 11144342]
28. Bauer SM, et al. Culture and the prevalence of hallucinations in schizophrenia. Compr Psychiatry. 2011; 52:319–325. [PubMed: 21497227]
29. Carlsson A. The current status of the dopamine hypothesis of schizophrenia. Neuropsychopharmacology. 1988; 1:179–186. [PubMed: 3075131]
30. Seeman P, Lee T. Antipsychotic drugs: direct correlation between clinical potency and presynaptic action on dopamine neurons. Science. 1975; 188:1217–1219. [PubMed: 1145194]
31. Earls LR, et al. Age-dependent microRNA control of synaptic plasticity in 22q11 deletion syndrome and schizophrenia. J Neurosci. 2012; 32:14132–14144. [PubMed: 23055483]
32. Stark KL, et al. Altered brain microRNA biogenesis contributes to phenotypic deficits in a 22q11-deletion mouse model. Nat Genet. 2008; 40:751–760. [PubMed: 18469815]
33. Ambros V. The functions of animal microRNAs. Nature. 2004; 431:350–355. [PubMed: 15372042]
34. Earls LR, Zakharenko SS. A Synaptic Function Approach to Investigating Complex Psychiatric Diseases. Neuroscientist. 2013; 20:257–271. [PubMed: 23907185]
35. Flurkey, K.; Currer, JM.; Harrison, DE. The Mouse in Aging Research. In: Fox, JG., et al., editors. The Mouse in Biomedical Research. American College Laboratory Animal Medicine (Elsevier); Burlington, MA: 2007. p. 637-672.
36. Smith PH, Populin LC. Fundamental differences between the thalamocortical recipient layers of the cat auditory and visual cortices. J Comp Neurol. 2001; 436:508–519. [PubMed: 11447593]

37. Swerdlow NR, Weber M, Qu Y, Light GA, Braff DL. Realistic expectations of prepulse inhibition in translational models for schizophrenia research. Psychopharmacology (Berl). 2008; 199:331–388. [PubMed: 18568339]
38. Braff DL, Geyer MA, Swerdlow NR. Human studies of prepulse inhibition of startle: normal subjects, patient groups, and pharmacological studies. Psychopharmacology (Berl). 2001; 156:234–258. [PubMed: 11549226]
39. Denzler R, Agarwal V, Stefano J, Bartel DP, Stoffel M. Assessing the ceRNA hypothesis with quantitative measurements of miRNA and target abundance. Mol Cell. 2014; 54:766–776. [PubMed: 24793693]
40. Small EM, Olson EN. Pervasive roles of microRNAs in cardiovascular biology. Nature. 2011; 469:336–342. [PubMed: 21248840]
41. Chun S, Bayazitov IT, Blundon JA, Zakharenko SS. Thalamocortical long-term potentiation becomes gated after the early critical period in the auditory cortex. J Neurosci. 2013; 33:7345–7357. [PubMed: 23616541]
42. Emptage NJ, Reid CA, Fine A, Bliss TV. Optical quantal analysis reveals a presynaptic component of LTP at hippocampal Schaffer-associational synapses. Neuron. 2003; 38:797–804. [PubMed: 12797963]
43. Richardson RJ, Blundon JA, Bayazitov IT, Zakharenko SS. Connectivity patterns revealed by mapping of active inputs on dendrites of thalamorecipient neurons in the auditory cortex. J Neurosci. 2009; 29:6406–6417. [PubMed: 19458212]
44. Conn PJ, Tamminga C, Schoepp DD, Lindsley C. Schizophrenia: moving beyond monoamine antagonists. Mol Interv. 2008; 8:99–107. [PubMed: 18403654]
45. Leucht S, et al. Second-generation versus first-generation antipsychotic drugs for schizophrenia: a meta-analysis. Lancet. 2009; 373:31–41. [PubMed: 19058842]
46. Miyamoto S, Miyake N, Jarskog LF, Fleischhacker WW, Lieberman JA. Pharmacological treatment of schizophrenia: a critical review of the pharmacology and clinical effects of current and future therapeutic agents. Mol Psychiatry. 2012; 17:1206–1227. [PubMed: 22584864]
47. Clinton SM, Meador-Woodruff JH. Thalamic dysfunction in schizophrenia: neurochemical, neuropathological, and in vivo imaging abnormalities. Schizophr Res. 2004; 69:237–253. [PubMed: 15469196]
48. Cronenwett WJ, Csernansky J. Thalamic pathology in schizophrenia. Curr Top Behav Neurosci. 2010; 4:509–528. [PubMed: 21312411]
49. Oke AF, Adams RN, Winblad B, von KL. Elevated dopamine/norepinephrine ratios in thalami of schizophrenic brains. Biol Psychiatry. 1988; 24:79–82. [PubMed: 3370279]
50. Wong DF, et al. Positron emission tomography reveals elevated D2 dopamine receptors in drug-naive schizophrenics. Science. 1986; 234:1558–1563. [PubMed: 2878495]
51. Abi-Dargham A, et al. Increased baseline occupancy of D2 receptors by dopamine in schizophrenia. Proc Natl Acad Sci U S A. 2000; 97:8104–8109. [PubMed: 10884434]
52. Behrendt RP. Hallucinations: synchronisation of thalamocortical gamma oscillations underconstrained by sensory input. Conscious Cogn. 2003; 12:413–451. [PubMed: 12941286]
53. Llinas RR, Pare D. Of dreaming and wakefulness. Neuroscience. 1991; 44:521–535. [PubMed: 1754050]
54. Welsh RC, Chen AC, Taylor SF. Low-frequency BOLD fluctuations demonstrate altered thalamocortical connectivity in schizophrenia. Schizophr Bull. 2010; 36:713–722. [PubMed: 18990709]
55. Woodward ND, Karbasforoushan H, Heckers S. Thalamocortical dysconnectivity in schizophrenia. Am J Psychiatry. 2012; 169:1092–1099. [PubMed: 23032387]
56. Woo PY, Leung LN, Cheng ST, Chan KY. Monoaural musical hallucinations caused by a thalamocortical auditory radiation infarct: a case report. J Med Case Rep. 2014; 8:400. [PubMed: 25468292]
57. Sobin C, Kiley-Brabeck K, Karayiorgou M. Associations between prepulse inhibition and executive visual attention in children with the 22q11 deletion syndrome. Mol Psychiatry. 2005; 10:553–562. [PubMed: 15520831]

58. Almeida OP, Howard RJ, Levy R, David AS. Psychotic states arising in late life (late paraphrenia) psychopathology and nosology. Br J Psychiatry. 1995; 166:205–214. [PubMed: 7728365]
59. Zhang J, Engel JA, Ericson M, Svensson L. Involvement of the medial geniculate body in prepulse inhibition of acoustic startle. Psychopharmacology (Berl). 1999; 141:189–196. [PubMed: 9952044]
60. Thaker GK, Carpenter WT Jr. Advances in schizophrenia. Nat Med. 2001; 7:667–671. [PubMed: 11385502]
61. Cruikshank SJ, Rose HJ, Metherate R. Auditory thalamocortical synaptic transmission in vitro. J Neurophysiol. 2002; 87:361–384. [PubMed: 11784756]
62. Blundon JA, Bayazitov IT, Zakharenko SS. Presynaptic gating of postsynaptically expressed plasticity at mature thalamocortical synapses. J Neurosci. 2011; 31:16012–16025. [PubMed: 22049443]
63. Boyden ES, Zhang F, Bamberg E, Nagel G, Deisseroth K. Millisecond-timescale, genetically targeted optical control of neural activity. Nat Neurosci. 2005; 8:1263–1268. [PubMed: 16116447]
64. Dweep H, Sticht C, Pandey P, Gretz N. miRWalk--database: prediction of possible miRNA binding sites by “walking” the genes of three genomes. J Biomed Inform. 2011; 44:839–847. [PubMed: 21605702]
65. Christensen M, Larsen LA, Kauppinen S, Schratt G. Recombinant Adeno-Associated Virus-Mediated microRNA Delivery into the Postnatal Mouse Brain Reveals a Role for miR-134 in Dendritogenesis in Vivo. Front Neural Circuits. 2010; 3:16. [PubMed: 20126250]
66. Kluiver J, et al. Rapid generation of microRNA sponges for microRNA inhibition. PLoS One. 2012; 7:e29275. [PubMed: 22238599]
67. Kluiver J, et al. Generation of miRNA sponge constructs. Methods. 2012; 58:113–117. [PubMed: 22836127]
68. Mellado Lagarde MM, et al. Spontaneous regeneration of cochlear supporting cells after neonatal ablation ensures hearing in the adult mouse. Proc Natl Acad Sci U S A. 2014; 111:16919–16924. [PubMed: 25385613]

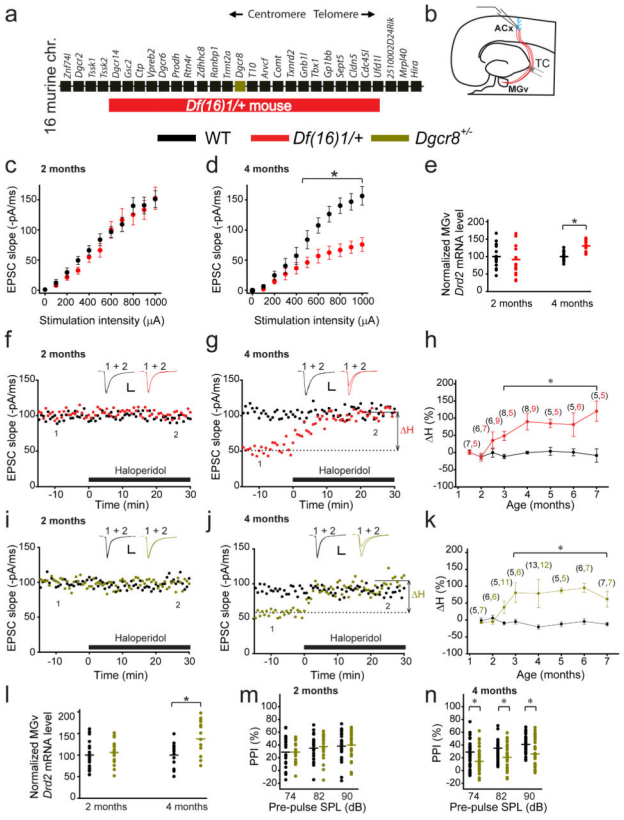

Fig. 1. Adult onset of antipsychotics sensitivity and synaptic transmission disruption in auditory TC projections of mouse models of 22q11DS

(**a**) Map of 22q11DS orthologs deleted in *Df(16)1/+* mice. (**b**) Illustration of voltage-clamp recordings of thalamorecipient L3/4 pyramidal neurons in TC slices. TC projections are shown in red. ACx, auditory cortex; TC, thalamocortical; MGv, ventral part of the medial geniculate nuclei. (**c**, **d**) Input–output relations between stimulation intensity and EPSCs at TC projections in the ACx of 2- (**c**, $F_{(1,37)}$=0.967, p=0.338) or 4-month-old (**d**, $F_{(1,46)}$=11.56, *p<0.001) WT (20 and 23 neurons, respectively) and *Df(16)1/+* mice (19 and 25 neurons, respectively). (**e**) *Drd2* transcript levels in the MGV of 2- and 4-month-old WT and *Df(16)1/+* mice (2 months: 6 mice of each genotype, measured in triplicates, U=126; p=0.261; 4 months: 5 mice of each genotype, measured in triplicates, $t_{(28)}$= –5.78; *p <0.001). (**f**, **g**) The effect of haloperidol on TC EPSCs in 2- (**f**) and 4-month-old (**g**) WT and *Df(16)1/+* littermates. Haloperidol-induced percentage change (ΔH) in the slope of TC EPSCs relative to baseline (before haloperidol application; dashed line). (**h**) The ΔH as a function of mouse age in WT and *Df(16)1/+* littermates. (**i**, **j**) The effect of haloperidol on TC EPSCs in 2- (**i**) and 4-month-old (**j**) WT and *Dgcr8*$^{+/-}$ littermates. (**f**, **g**, **i**, **j**) Scale bars, 50 pA, 10 ms. Insets show representative EPSCs before (1) and after (2) haloperidol application. (**k**) The ΔH as a function of mouse age in WT and *Dgcr8*$^{+/-}$ littermates. (**h**, **k**) The number of cells recorded at each age is shown in parentheses above the plots. *p <0.01 (two-tailed *t*-test or Mann-Whitney Rank Sum *U* test). (**l**) Average *Drd2* mRNA levels normalized to *Gapdh* in the auditory thalamus of 2- and 4-month-old WT and *Dgcr8*$^{+/-}$ littermates (2 months: 7 mice of each genotype; 4 months: 4 WT mice, 5 *Dgcr8*$^{+/-}$ mice,

measured in triplicates).The $t_{(24)}$=−2.44; *p=0.022, two-tailed *t*-test. (**m**, **n**) Mean PPI of maximal acoustic-startle response in 2- (**m**) and 4-month-old (**n**) WT and *Dgcr8*$^{+/-}$ littermates (2 months: 23 WT mice and 22 *Dgcr8*$^{+/-}$ mice; 4 months: 36 WT mice and 41 *Dgcr8*$^{+/-}$ mice). *p <0.05 (two-tailed *t*-test or Mann-Whitney Rank Sum *U* test). SPL (sound pressure level). (**c, d**, **h**, **k**, **m**, **n**) Data are represented as the mean ± SEM. (**e**, **l–n**) Horizontal lines represent the mean values.

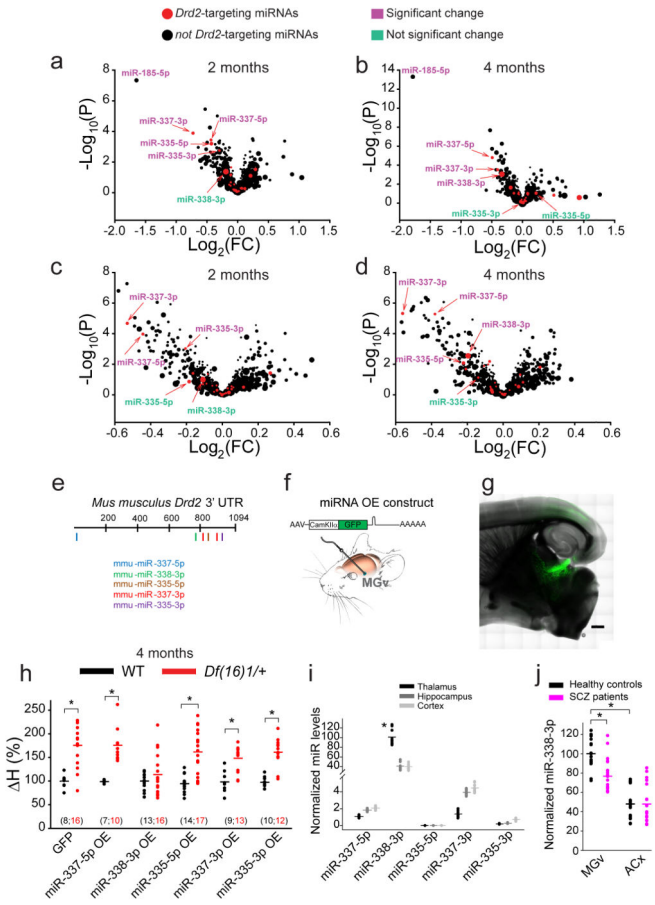

Fig. 2. Identification of *Drd2*-targeting miR-338-3p in the auditory thalamus

(**a–d**) Volcano plots of miRNA microarray data from the auditory thalamus of 2- (**a**, **c**) and 4-month-old (**b**, **d**) WT and *Df(16)1/+* (**a**, **b**) and WT and *Dgcr8*$^{+/-}$ (**c**, **d**) male littermates. The difference between miRNA levels in WT and mutants was considered significant if p <0.01. Symbol size represents the miRNA expression level in the microarray. Note, miR-338-3p had the highest expression among all predicted *Drd2*-targeting miRNAs. (**e**) Diagram of the mouse *Drd2* 3′UTR (XM_006509996.2) with seed sites for the 5 miRNAs indicated. (**f**) Experimental design of a recombinant AAV encoding a chimeric construct overexpressing an miRNA of interest (top) injected into the mouse MGv (bottom). (**g**) GFP expressed specifically in the auditory TC projections after in vivo injection of recombinant AAV. Scale bar, 500 μm. (**h**) Haloperidol sensitivity of TC projections in 4-month-old WT and *Df(16)1/+* mice injected with AAVs encoding different miRNAs or GFP. The number of cells recorded is shown in parentheses. *p <0.01 (two-tailed *t*-test or Mann-Whitney Rank Sum *U* test). (**i**) Relative average levels of miRNA expression in the thalamus, hippocampus, and cortex of WT mice (5 mice, run in triplicates). Data normalized to the average of three housekeeping genes: U6, snoRNA202, and snoRNA234. Only miR-338-3p shows enrichment in the thalamus. $H_{(2)}$=18.85, *p <0.001. (**j**) Mean relative miR-338-3p levels (normalized to *U6*) in the postmortem MGv and ACx tissues from healthy controls and patients with schizophrenia (SCZ) (MGv: 7 controls and 7 patients ($t_{(40)}$=4.56; *p <0.001); ACx: 8 controls and 8 patients (*U*=278; p=0.845), measured in triplicates). *p <0.05.

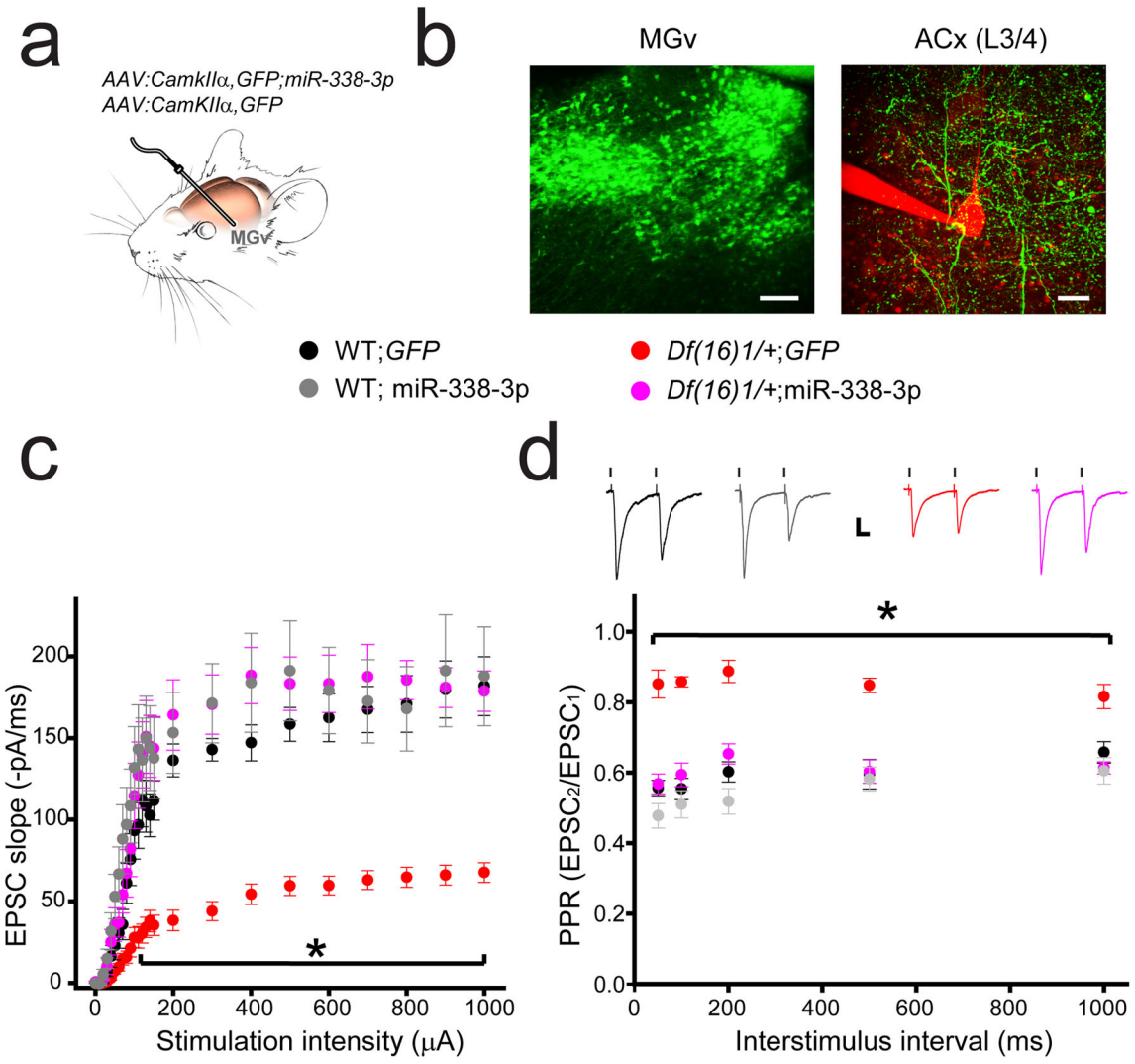

Fig. 3. Replenishment of miR-338-3p in the auditory thalamus rescues deficits in synaptic transmission and presynaptic neurotransmitter release at TC projections of 22q11DS mouse models

(**a**) In vivo infection of MGv relay neurons with *AAV-GFP-miR-338-3p or AAV-GFP.* (**b**) GFP expression (green) in cell bodies in the MGv (left; scale bar, 100 μm) and in projections to the thalamorecipient L3/4 layer of the ACx (right; scale bar, 20 μm). A patch pipette and part of an L3/4 pyramidal neuron filled with Alexa 594 are shown in red. (**c**, **d**) Input–output relations between stimulation intensity and EPSCs (**c**) and PPR (**d**) at TC projections in the ACx of 4- to 5-month-old WT and *Df(16)1/+* mice injected with either *AAV-GFP-miR-338-3p* or *AAV-GFP.* Insets show representative EPSCs. Scale bar, 20 ms, 50 pA. (**c**) 16 WT;GFP neurons, 10 WT; miR-338-3p neurons, 20 *Df(16)1/+*;GFP neurons, 13 *Df(16)1/+*; miR-338-3p neurons. $F_{(3,24)}$=268.7, *p<0.001. (**d**) 17 WT;GFP neurons, 12 WT; miR-338-3p neurons, 19 *Df(16)1/+*;GFP neurons, 14 *Df(16)1/+*; miR-338-3p neurons. $F_{(3,4)}$=107.2, *p<0.001. Data are represented as the mean ± SEM.

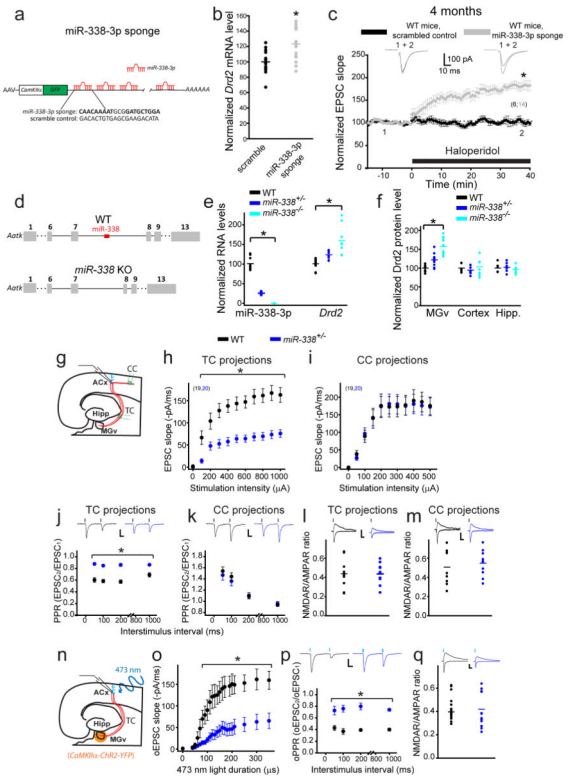

Fig. 4. The depletion or knockout of *miR-338* replicates the TC deficiency of *Df(16)1/+* mice

(**a**) AAV expressing an miR-338-3p sponge construct with multiple binding sites to miR-338-3p in the GFP 3′UTR, under control of the *CamKIIα* promoter. Sequences for the miR-338-3p sponge and the scrambled control are shown below. Bold text indicates seed-site sequence. (**b**) Relative *Drd2* mRNA levels after infection of MGv excitatory neurons in WT mice with an AAV encoding a scrambled control (5 mice, run in triplicates) or miR-338-3p sponge (6 mice, run in triplicates), U=53, *p=0.005. (**c**) Normalized mean TC EPSCs before and after application of haloperidol in WT mice after infection of MGv neurons with AAVs encoding a scrambled control (6 neurons) or miR-338-3p sponge (14 neurons). Insets show representative EPSCs. *p <0.001 (two-tailed *t*-test). (**d**) Generation of *miR-338* knockout (KO) mice. (**e**) Normalized levels of miR-338-3p and *Drd2* in the auditory thalamus of WT (miR-338-3p: 3 mice, *Drd2:* 5 mice), *miR-338*$^{+/-}$ (miR-338-3p: 4 mice, *Drd2:* 6 mice) and *miR-338*$^{-/-}$ mice (miR-338-3p: 4 mice, *Drd2:* 4 mice). Run in triplicates. miR-338-3p: $H_{(2)}$=26.5, *p <0.001; *Drd2:* $H_{(2)}$=25.2, *p <0.001. (**f**) Normalized levels of Drd2 protein in the auditory thalamus ($H_{(2)}$=23.3, *p<0.01), cortex ($H_{(2)}$=1.21, p=0.544), and hippocampus (Hipp.) ($t_{(2)}$=0.4, p=0.674) of WT (3 mice), *miR-338*$^{+/-}$ (4 mice), and *miR-338*$^{-/-}$ mice (4 mice). Run in duplicates or triplicates. (**g**) Simultaneous recordings of EPSCs in L3/4 pyramidal neurons evoked by electrical stimulation of the thalamocortical (TC) and corticocortical (CC) projections. (**h**, **i**) Input–output relations between electrical stimulation intensity and EPSCs at TC projections (**h**, $F_{(1,37)}$=26.9, *p <0.001) and CC projections (**i**, $F_{(1,37)}$=0.002, p=0.964) in the ACx of 4-month-old WT mice (19 neurons) and *miR-338*$^{+/-}$ mice (20 neurons). PPR ratio (**j**, **k**) and NMDAR/AMPAR ratio (**l**, **m**) of electrically evoked EPSCs measured at TC projections (**j**, **l**) and CC

projections (**k**, **m**) of 4-month-old WT (26, 23, 10, 9 neurons, respectively) and *miR-338*$^{+/-}$ mice (22, 19, 12, 10 neurons, respectively). (**j**) *p <0.001 (two-tailed *t*-test); (**k**) p >0.05 (two-tailed *t*-test); (**l**) $t(20)$=0.03, p=0.974; (**m**) $t(17)$=–0.576, p=0.572. (**n**) Optogenetic experiments in TC slices. ChR2 was expressed in the MGv, under control of the *CamKIIα* promoter. (**o–q**) Input–output relations (**o**), PPR (**p**), and NMDAR/AMPAR ratio (**q**) of optically evoked EPSCs (oEPSC) measured at TC projections of 4-month-old WT (10, 16, 14 neurons, respectively) and *miR-338*$^{+/-}$ mice (9, 16, 17 neurons, respectively). (**o**) $F_{(1,17)}$=11.25, *p=0.004; (**p**) *p <0.001 (two-tailed *t*-test); (**q**) U=98, p=0.296. Insets show representative AMPAR-mediated (–70 mV holding membrane potential) and NMDAR-mediated (+40 mV holding membrane potential) EPSC and oEPSC traces. Scale bars, 20 ms, 50 pA. (**c**, **h–k**, **o**, **p**) Data are represented as the mean ± SEM. (**b**, **e**, **f**, **l**, **m**, **q**) Horizontal lines represents the mean values. *p <0.01.

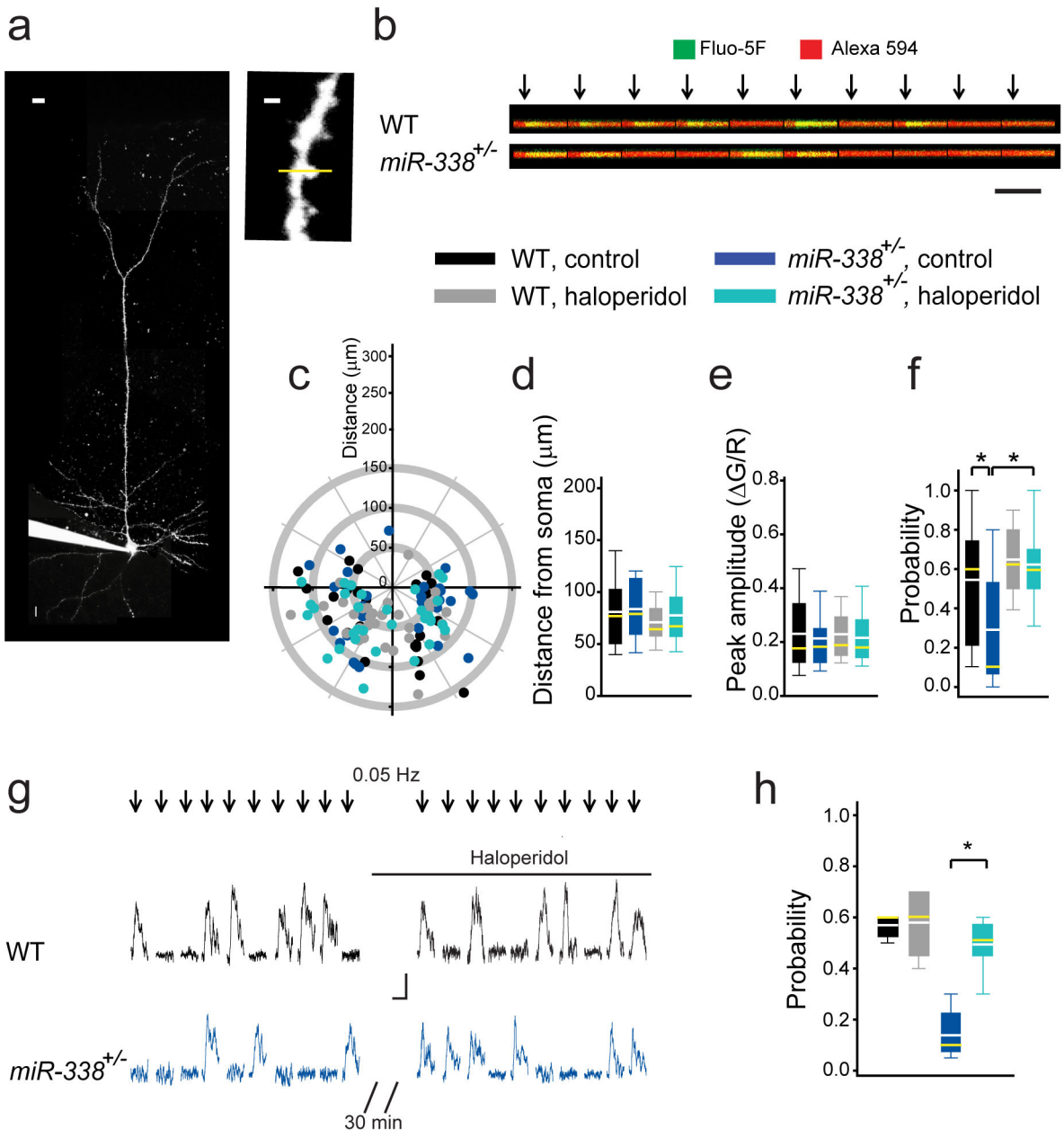

Fig. 5. Probability of glutamate release is reduced at TC projections of *miR-338*$^{+/-}$ mice

(**a**) An L3/4 pyramidal neuron filled with Fluo-5F and Alexa 594 through a patch pipette (left; scale bar, 10 µm) to visualize synaptically evoked calcium transients inside dendritic spines (right; scale bar, 1µm). Yellow line represents the line scan. (**b**) Calcium transients in a dendritic spine in response to a single thalamic stimulation (arrows) repeated 10 times at 0.05–0.1 Hz. Scale bar, 0.1 ΔG/R, 200 ms. (**c**) Location of active TC inputs on dendritic trees of L3/4 pyramidal neurons spines. (0;0), soma coordinates (apical dendrites pointing upwards). (**d–f**) Average distances from the soma to active TC inputs (**d**), calcium transient peak amplitudes (**e**), and probabilities (**f**) in response to 10 to 20 single TC stimulations in WT and *miR-338*$^{+/-}$ slices not treated (WT: 27 spines; *miR-338*$^{+/-}$: 32 spines) or treated

(WT: 32 spines; *miR-338*$^{+/-}$: 41spines) with haloperidol. (**d**) $F_{(3)}$=1.05, p=0.373; (**e**) $H_{(3)}$=0.644, p=0.886; (**f**) $H_{(3)}$=31.51, *p <0.001. (**g**, **h**) Representative traces (**g**) and average probability (**h**) of calcium transients in the same dendritic spines before and after haloperidol application in WT (5 spines) and *miR-338*$^{+/-}$ mice (9 spines). $H_{(3)}$=14.5, *p=0.002. (**d–f**, **h**) Data are represented as the mean (white lines), median (yellow lines), 10th, 25th, 75th, and 90th percentiles.

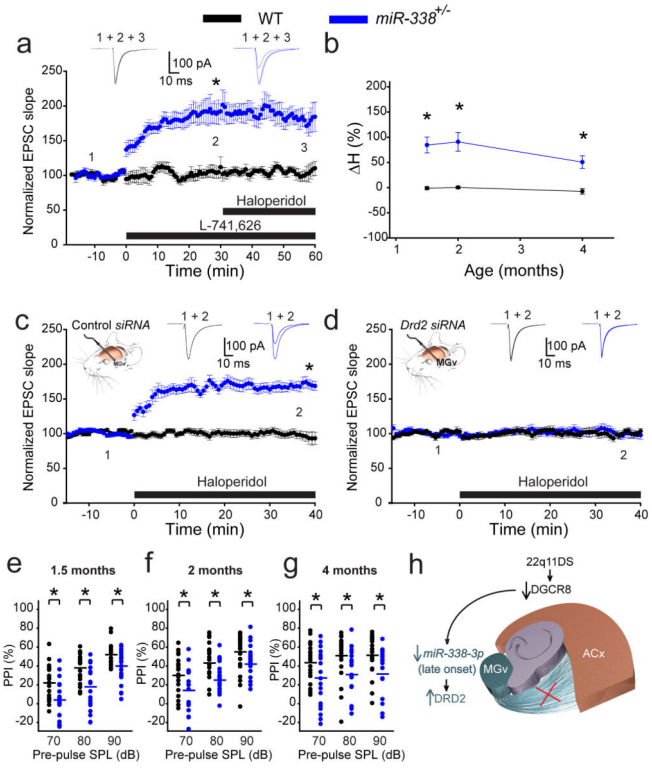

Fig. 6. Deletion of *miR-338* in mice eliminates age dependency for antipsychotics sensitivity and replicates 22q11DS phenotypes

(**a**) Average TC EPSCs before (1) and during (2–3) application of the Drd2-specific inhibitor L-741,626 and haloperidol in 4-month-old WT (6 neurons) and *miR-338*$^{+/-}$ mice (9 neurons). (**b**) Mean haloperidol sensitivity (ΔH) in WT (10, 7, 6 neurons at 1.5, 2, and 4 months, respectively) and *miR-338*$^{+/-}$ mice (12 neurons at each age) between 1.5 and 4 months of age. *p <0.001 (two-tailed *t*-test). (**c**, **d**) Mean TC EPSCs before (1) and after (2) haloperidol in 2-month-old WT (10 control siRNA neurons and 9 *Drd2* siRNA neurons) and *miR-338*$^{+/-}$ mice (14 control siRNA neurons and 10 *Drd2* siRNA neurons) that received control (**c**) or *Drd2* siRNA injected into their MGv (**d**). Insets show representative EPSCs. (**e**–**g**) Mean PPI of maximal acoustic startle response in 1.5- (**e**), 2- (**f**), and 4-month-old (**g**) WT (22, 22, 21 mice, respectively) and *miR-338*$^{+/-}$ littermates (21, 21, 20 mice, respectively). (**e**) $F_{(5)}$=21.648, *p<0.001; (**f**) $H_{(5)}$=39.887, *p<0.001; (**g**) $H_{(5)}$=17.348, *p=0.004. SPL, sound pressure level. (**h**) Model of TC disruption in 22q11DS. DGCR8-dependent depletion of the thalamus-enriched miR-338-3p leads to an increase in DRD2 level in the auditory thalamus (MGv) and disruption of thalamocortical synaptic transmission to the auditory cortex (ACx) later in life.